Proc. Natl. Acad. Sci. USA
Vol. 88, pp. 7046–7050, August 1991
Biophysics

Static and statistical bending of DNA evaluated by Monte Carlo simulations

(DNA curvature/anisotropy of DNA bending/fluctuations in B-DNA/conformational energy calculations)

V. B. ZHURKIN*†, N. B. ULYANOV†, A. A. GORIN†, AND R. L. JERNIGAN*

*Laboratory of Mathematical Biology, National Cancer Institute, National Institutes of Health, Building 10, Room 4B-56, Bethesda, MD 20892; and †The Engelhardt Institute of Molecular Biology, Academy of Sciences of the U.S.S.R., 117 984 Moscow B-334, Vavilov str. 32, U.S.S.R.

Communicated by I. Tinoco, Jr., May 6, 1991

ABSTRACT **To investigate the influence of thermal fluctuations on DNA curvature the Metropolis procedure at 300 K was applied to B-DNA decamers containing $A_5 \cdot T_5$ and $A_4 \cdot T_4$ blocks. Monte Carlo simulations have confirmed the DNA bending anisotropy: B-DNA bends most easily in a groove direction (roll). The $A_5 \cdot T_5$ block is more rigid than the other sequences; the pyrimidine–purine dimers are found to be the most flexible. For A_5TCTCT, A_5CTCTC, and A_5GAGAG, the average bend angle per decamer is 20–25° in a direction toward the minor groove in the center of the $A_5 \cdot T_5$ tract, which is consistent with both the "junction" and "wedge AA" models. However, in A_5T_5, A_4T_4CG, and T_4A_4GC, bending is directed into the grooves at the 5′ and 3′ ends of purine tracts. Thus, directionality of bending caused by $A_n \cdot T_n$ blocks strongly depends on their neighboring sequences. These calculations demonstrate that the sequence-dependent variation of the minor-groove width mimics the observed hydroxyl radical cleavage pattern. To estimate the effect of fluctuations on the overall shape of curved DNA fragments, longer pieces of DNA (up to 200 base pairs) were generated. For sequences with strong curvature (A_5X_5 and A_4T_4CG), the static model and Monte Carlo ensemble give similar results but, for moderately and slightly curved sequences (A_5T_5 or T_4A_4GC), the static model predicts a much smaller degree of bending than does the statistical representation. Considering fluctuations is important for quantitative interpretation of the gel electrophoresis measurements of DNA curvature, where both the static and statistical bends are operative.**

The intrinsic bending (or curvature) of DNA is closely related to numerous biological processes—e.g., packaging in chromatin, gene regulation, and recombination (for reviews, see refs. 1–3). The curved DNA sequences demonstrate anomalously slow migration in polyacrylamide gel electrophoresis experiments. Several models were suggested recently (4–6) to quantitatively describe this phenomenon. These models neglect thermal fluctuations and deal with some static parameters, "junction" angles (4) or the "wedge" angles (1, 6). Whereas the junction model phenomenologically describes bending of DNA containing $A_n \cdot T_n$ blocks, the two wedge models (5, 6) claim to predict curvature of DNA with an arbitrary sequence at the base step level; however, they differ significantly in the values of the wedge angles. In our view, there are two shortcomings to that approach. (*i*) The wedge angles are comparable to or smaller than the corresponding fluctuations, estimated as 5–7° based on the persistence length of DNA as 500 Å (7). (*ii*) There is an asymmetry in DNA bending: it bends to different extents into the minor and major grooves (8–10), so the average bend angle can deviate significantly from the energetically optimal one.

The publication costs of this article were defrayed in part by page charge payment. This article must therefore be hereby marked "*advertisement*" in accordance with 18 U.S.C. §1734 solely to indicate this fact.

The problem of averaging is not trivial in this case. Direct use of the averages of the microscopic parameters does not necessarily produce an adequate description of the macroscopic shape of curved DNA. Indeed, parameters defining the overall DNA shape, such as the end-to-end distance, depend on the sum of the wedge vectors and, generally, the average of the sum does not equal the sum of averages.

The questions to be addressed here are as follows: How do the local fluctuations of DNA influence the macroscopic shape of the curved DNA fragments? And how does this influence depend on sequence? We have undertaken Monte Carlo (MC) simulations of decameric duplexes containing $A_n \cdot T_n$ runs, observed to produce a large DNA curvature (11, 12). In previous studies of DNA bending, either certain restrictions were imposed on the duplex boundaries (8, 13) or dimers with free ends were considered (14). In the recent thermodynamic sampling studies (9, 10), only base–base stacking interactions were calculated and the base-pair geometries were described by reduced sets of parameters.

Here we consider all essential degrees of freedom in the double helix, including base pairs and sugar-phosphate backbones. The decamer structures were generated with periodic boundary conditions, so they could be combined to produce longer pieces of DNA. In this way we avoided both the free ends and the fixed boundaries, each of which could cause artifacts. We restricted ourselves to double-helical forms from the B-DNA family that dominate under standard conditions. Consideration of only a set of similar DNA conformations has an additional advantage since relative orientations of hydrated groups remain practically unchanged and, therefore, *in vacuo* energy calculations are more physically meaningful.

METHODS

The Metropolis procedure (15) at 300 K was used to study the eight decamers: $(A_5T_5)_2$, A_5TCTCT·AGAGAT$_5$, A_5CTCTC·GAGAGT$_5$, A_5GAGAG·CTCTCT$_5$, $A_{10} \cdot T_{10}$, $(AG)_5 \cdot (CT)_5$, A_4T_4CG·CGA_4T_4, and T_4A_4GC·GCT_4A_4. The sequences are chosen so that the $A_5 \cdot T_5$ blocks were surrounded by different nucleotides; the last two decamers differ significantly in their degree of curvature (16).

The generalized coordinates of bases and sugar rings are taken as independent variables of the system. They are as follows: six parameters for the step (wedge) from one base pair to the neighboring base pair [three rotations and three translations (17)], six independent variables within each base pair (17), pseudorotational phase angles *P* of the sugar rings and the glycosidic angles. In all, the system has 160 independent variables. Geometry of the sugar-phosphate backbone was found with the use of the chain-closure algorithm, developed in this laboratory (18). All the dihedral angles remain within the limits of the B-family; their variations about

Abbreviation: MC, Monte Carlo.

mean values do not exceed 14°. The average values of the deoxyribose pseudorotation angle P equal 135–158° for purines and 124–140° for pyrimidines; fluctuation ΔP is 11–17° depending on sequence.

The Markov chains were created in the following way: first, the decamer structures were minimized, then temperature was gradually increased up to 300 K and 60,000 iterations were made to equilibrate the system; after that the Boltzmann ensemble obtained in the course of 10^5 iterations was used to calculate the averages and root-mean-square fluctuations denoted by Δ.

The energies were calculated with the use of the atom–atom potentials (19, 20). The phosphate groups were electroneutral (21); therefore, interactions of a nucleotide with only the closest neighbors were taken into account. The data are presented for the distance dependence of dielectric constant $\varepsilon(r) = r$; we found results practically unchanged when $\varepsilon = 4$ was used. The DNA structures with the minor groove width less than 6 Å were excluded from the Boltzmann ensemble [the groove width is calculated as the lowest phosphorus–phosphorus (P–P) distance]. In all the structures reported here, the average winding varies from 35.5° to 36.5°.

The structure of $A_n{\cdot}T_n$ blocks is characterized by a narrow minor groove (22); the ordered water spine is conceivably among the factors stabilizing this structure (23). To model the influence of solvent, the pseudoenergy term is added, estimating deviations of H–H distances from the NMR measurements (24, 25): $E = \Sigma_i\, C(r_i - r_i^\circ)^2$, where $r_i^\circ = 3.65$ Å for the AdeH2 · · · H1'Thy distance and 3.80 Å for AdeH2 · · · H1'Ade, and $C = 3$ kcal·mol^{-1}·Å^{-2}. For the chosen energy constants the average values and fluctuations are 3.80 ± 0.24 Å for the first distance and 4.05 ± 0.27 Å for the second.

The decamers were generated with periodic boundary conditions. For instance, for A_5TCTCT, the dodecamer TCTA$_5$TCTC was actually considered, with the geometries of the last two nucleotides, TC, always taken to be identical to those of the first TC. This device allowed us to introduce a simple and unambiguous notion of the bending angle β per decamer (Fig. 1). To compare the static and statistical descriptions of DNA bending, two values were calculated: the bending angle β averaged over the MC ensemble of decamer structures and the "static" bend β_s obtained in the same way as in Fig. 1 but for the average parameters of all dimeric steps (wedges) (Table 1).

Selecting periodic sequences and periodic boundaries enabled us to generate and analyze the longer bent fragments of DNA. For this purpose the dodecamer structures were chosen randomly from the Boltzmann ensemble of 10^5 structures, and vectors from the 1st to 11th base pair were used to build up a new segment in the growing chain. In this way 5×10^4 DNA fragments up to 200 base pairs (bp) in length were generated and parameters describing their shape were calculated (see Fig. 5).

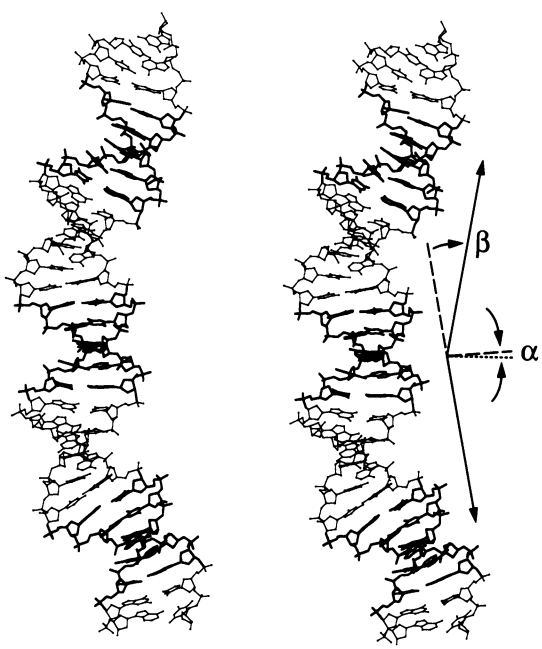

FIG. 1. Definition of bending angle, β, and direction of bending, α. Typical snapshot of the decamer A_5CTCTC, repeated three times. The decamers are generated with periodic boundary conditions, so they can be extended to demonstrate a noticeable curvature of DNA. To define the α and β angles, the geometrical centers of A·T pairs in the center of $A_5{\cdot}T_5$ blocks (emphasized) are connected by vectors (shifted to the right for clarity). The bisecting vector is projected on the plane of the central A·T pair (dashed line), and the angle between this line and the dyad axis of the A·T pair (dotted line) defines direction of bending, α (for A_5CTCTC, $\alpha \approx 0$).

RESULTS

Sequence Dependence of the B-DNA Fluctuations. The roll angle was found to be the most flexible among the angle parameters of the DNA wedges. Its fluctuation, $\Delta\rho$, varies from 4.4 to 9.1° depending on the nucleotide sequence; whereas the fluctuation in tilt ($\Delta\tau$) is 3.0–4.7°. So, MC simulations confirm the double-helix bending anisotropy revealed earlier by energy minimization (8, 13). These ranges for roll and tilt fluctuations are similar to those calculated for base stacking fluctuations alone (9, 10).

Fluctuations in the DNA winding angle ($\Delta\Omega$) of 2.3–4.5° agree well both with the theoretical estimations [energy minimization (21, 26) and molecular dynamics (27)] and with the data based on the DNA cyclization experiments (28, 29).

On the whole, the pyrimidine–purine dimers proved to be the most flexible ones, which correspond to the weakest overlap of bases (31). The A_5 block is more rigid than the other oligopurine blocks: $\Delta\rho$ is 4.4–6.5° for A_5 and $\Delta\rho$ is 5.7–8.3° for the alternating AG.

Directionality of DNA Bending and the Roll Angles. Consider A_5T_5 and A_5CTCTC (Fig. 2). The greatest difference between the roll values is found for the pyrimidine–purine dimers TA and CA on the one hand and AA, AT, and AC on the other hand. In accord with our energy minimization study (8), TA bends toward the major groove [positive roll (17)] and AT and AA bend toward the minor groove (negative roll). As a consequence, the decamer A_5T_5 is bent toward the major groove at the 5′ end of A_5 track, which is consistent with the pyrimidine–purine model (8, 32) and the chemical symmetry of this decamer. In our notation, the direction of bending (α) is 90° for A_5T_5 (Fig. 1). A_5T_5 reveals a "moderate" curvature: the average bending angle β is 14.8°, whereas the "static" bend β_s equals only 2.9° (Table 1).

Table 1. Bend angles for eight decamers

	β_s	β	$(\Delta\beta)$
A_5TCTCT·AGAGAT$_5$	20.7	26.0	(11.4)
A_5CTCTC·GAGAGT$_5$	20.2	25.8	(11.7)
A_5GAGAG·CTCTCT$_5$	19.6	24.9	(10.7)
A_4T_4CG·CGA_4T_4	14.3	19.2	(10.6)
T_4A_4GC·GCT_4A_4	6.0	15.5	(8.2)
$(A_5T_5)_2$	2.9	14.8	(8.0)
$(AG)_5{\cdot}(CT)_5$	1.6	17.1	(9.4)
$A_{10}{\cdot}T_{10}$	0.9	14.4	(7.8)

Static bend angles β_s are obtained as in Fig. 1 for the base-pair step parameters (three rotations and three translations) averaged over the MC ensemble of decamer structures. β and $(\Delta\beta)$ represent the mean value and thermal fluctuation (at 300 K) of the bend angle calculated individually for each decamer structure.

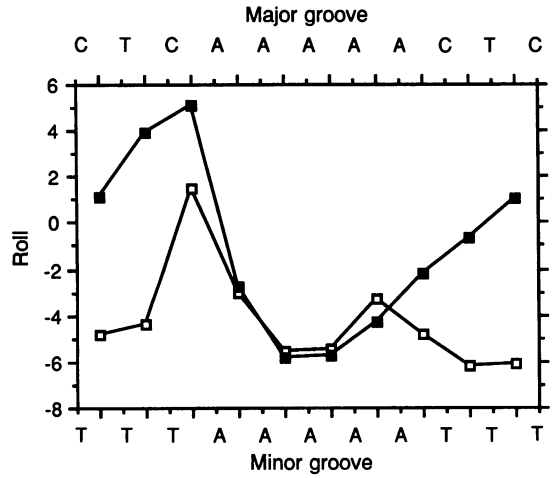

FIG. 2. Sequence dependence of the average roll angle ρ for A_5T_5 (open squares, with the sequence given on lower axis) and A_5CTCTC (solid squares, with sequence given on upper axis).

For A_5CTCTC all the four AA dimers have negative roll $\rho \approx -5°$, lower than all other dimers (Fig. 2), and this difference produces strong overall bending of A_5CTCTC toward the minor groove at the center of $A_5{\cdot}T_5$ (Fig. 1). In this case, direction of bending is $\alpha \approx 0$, which conforms with both the junction (2, 4, 12) and wedge AA models (6, 33). A very similar picture was obtained for the other two A_5X_5 decamers, A_5TCTCT and A_5GAGAG; they are bent essentially in the same direction, α is 0–15°. The average bend β equals 25–26°, and the "static" bend β_s is 20–21° for the three decamers (Table 1). The above values of β and β_s are consistent with the estimations made by Ulanovsky *et al.* (34) and Koo *et al.* (35) on the basis of the cyclization experiments.

So, in accord with the electrophoretic data (4, 12, 36, 37), the A_5X_5 decamers are bent significantly more strongly than A_5T_5. Directionality of their bending also differs dramatically.

Width of the Minor Groove. The dependence of the calculated minor groove width on sequence is remarkably consistent with the hydroxyl radical cleavage pattern, obtained by Burkhoff and Tullius (38) for the kinetoplast DNA: the groove is largest near the 5′ end of the A_n run and smallest at the 3′ end (Fig. 3). We explain this in the following way. In B-DNA the phosphorus atoms P(i) and P′(i − 4) are closest to each other across the minor groove (39); here P(i) and P′(i) denote the complementary nucleotides. This is shown for the sequence $X_5A_5{\cdot}T_5Y_5$ in the scheme below, where the lines depict closest distances across the groove and X and Y are any base:

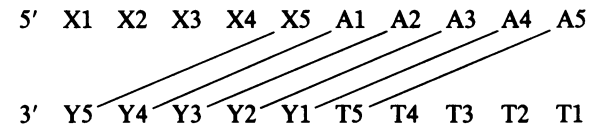

At A5 the groove width is given by the vector P′(T5)–P(A5), which spans the whole block $A_5{\cdot}T_5$. The oligo(dA)·oligo(dT) sequence is characterized by large propeller twist and small rise, and as a consequence the groove is relatively narrow here (39).

At A1 the groove width, g(A1), is measured between P(A1) and P′(Y4), so it is defined by geometry of the X2–X3–X4–X5–A1 block. The groove is essentially wider here than in $A_5{\cdot}T_5$; thus, g(A1) > g(A5). When moving from A1 to A5, the effect of $A_n{\cdot}T_n$ block accumulates, and the groove gradually narrows.

If the block X_5 is T_5, then the vector defined by P(A2)–P′(Y3) = P(A2)–P′(A3) spans the TTAA junction, which is opened into the minor groove (Fig. 2) and, hence, has the increased width of this groove. So, the minor groove is widest at A2 and A3.

As follows from the scheme above, for the symmetric sequences certain rules should be valid. For example, for A_5T_5 the equation g(A2) = g(A3) holds true, since in this case X = T, Y = A, and the groove is measured between P(A2) and P′(A3) or between P(A3) and P′(A2). Thus, A2 and A3 are equivalent. Similarly, g(A1) = g(A4), g(T2) = g(T3), g(T1) = g(T4), g(A5) = g(T5). Our data for A_5T_5 are consistent with these rules, in particular g(A2) = g(A3) (see Fig. 3). This provides a check on the sampling in our MC procedure, since all base pairs and wedge parameters were considered independently, and there were no imposed conditions implying symmetry of the sequence.

Comparison of A_4T_4CG and T_4A_4GC. These two decamers make up a classical example of the "strongly" and "slightly" curved molecules of DNA (16). It is interesting to compare their static and flexible (statistical) descriptions.

The static bend β_s equals 14.3° for A_4T_4CG and 6.0° for T_4A_4GC (Table 1). The circle diagrams in Fig. 4 help explain why A_4T_4CG is curved more significantly than T_4A_4GC. In the first case, all roll vectors in the center of the diagram are directed essentially in the same direction $\alpha = 90 \pm 36°$, whereas in T_4A_4GC they are directed at both $\alpha = 90 \pm 36°$ and $\alpha = 270 \pm 36°$, thereby compensating each other. This leads to a zig-zag path of the DNA axis and, as a consequence, to only a slight curvature of T_4A_4GC. Both decamers are bent along the dyad axis consistently with the symmetry of their sequences: the bending direction for A_4T_4CG is $\alpha = 90°$ and for T_4A_4GC is $\alpha = 270°$ (Fig. 4).

The periodic boundary conditions with which the decamers were generated imply that decamers can be extended by "ligating" one to another, thus creating a long superhelical fragment of DNA. Its shape can be described by the "width" of the curve d-max (40) measured as the maximum distance of a base-pair center from the straight line, connecting the first and the last base-pair centers (Fig. 5). Note that, although T_4A_4GC is bent much less than A_4T_4CG, the shape of its multimers deviates significantly from the straight line (obviously, d-max would be zero for a straight fragment).

When the fluctuations in decamers are considered, the description of their bending becomes rather different from the static picture. The average values of the bending angle β increase up to 19.2° and 15.5° for A_4T_4CG and T_4A_4GC, respectively, but this small difference in β does not reflect the striking contrast between them. Note that for the "straight" decamers $A_{10}{\cdot}T_{10}$ and

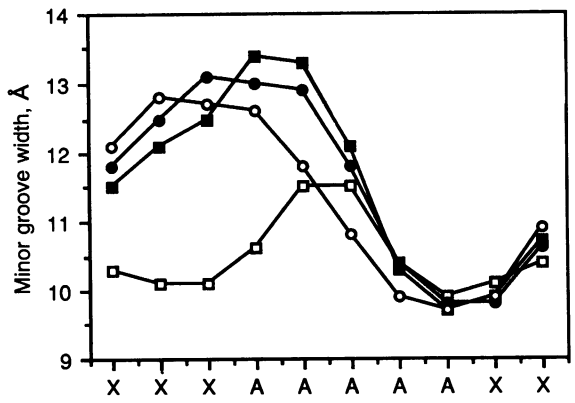

FIG. 3. Variation of the minor groove width in the decamers A_5CTCTC (■), A_5TCTCT (●), A_5GAGAG (○), and A_5T_5 (□). The groove width is measured as the average distance between the closest phosphorus atoms across the groove, P(i) and P′(i − 4). Thermal fluctuation of the groove size varies from 0.9 to 1.5 Å, the larger fluctuations corresponding to the wider groove.

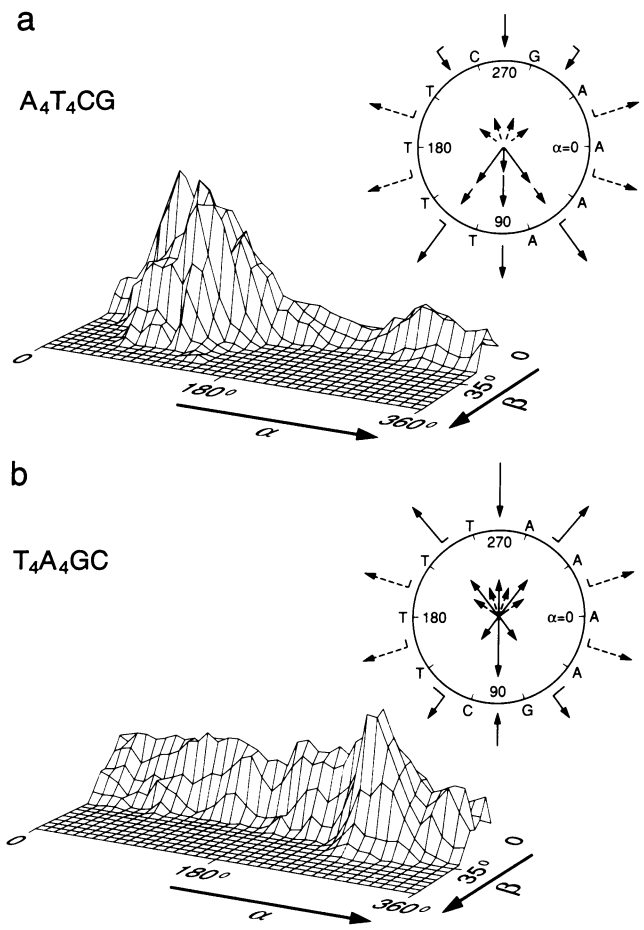

FIG. 4. Distribution of DNA bending in coordinates α (direction of bending) and β (bending angle) for A_4T_4CG (*a*) and T_4A_4GC (*b*). Circle diagrams of DNA bending (33, 37) with planes perpendicular to the helical axis are shown. Decamer sequence in 5′ → 3′ direction is given clockwise. Vectors outside the circle depict average roll and tilt components of the wedge angles obtained in the course of MC sampling: rolls are going along the radii and tilts are perpendicular to the radii. The AA·TT, AT, and AG·CT dimers are bent toward the minor groove (vectors going from the center), and TA, CG, GC, and GA·TC are bent toward the major groove (vectors pointing inward). The largest rolls are as follows: ρ(AA) = ρ(TT) = −5°, ρ(TA) = 8°; the average tilt angles do not exceed ±2° (AA·TT, AG·CT, and GA·TC are bent toward purines). The total bend per decamer can be calculated approximately as a sum of individual roll and tilt vectors (5, 33) (see the center of the circle). Thus, the bending direction for A_4T_4CG is α = 90° and for T_4A_4GC is α = 270°. The AA and TT roll vectors canceling each other are given in dashed lines; they are not shown in the circle's center. Probability [$p(\alpha, \beta)$] diagrams of bending in the direction α by angle β are also shown. The largest value of p for A_4T_4CG is p(75, 22.5) = 1.63%, for T_4A_4GC is p(275, 22.5) = 1.33%. The (α, β) plane is divided into 36 × 15 = 540 rectangles (increments in α are 10° and in β are 5°), so the average p = 0.2%.

$(AG)_5$·$(CT)_5$, the angle β equals 14–17° (Table 1), so that the β value *per se* cannot be used to distinguish between curved and straight fragments; to do so it is necessary to consider the directionality of bending as well.

The two-dimensional $p(\alpha, \beta)$ distribution of bending of A_4T_4CG (Fig. 4) shows that direction of its bending is localized primarily at $\alpha \approx 90°$, so that 65% of all molecules in the Boltzmann ensemble are bent in the interval $\alpha = 90 \pm 45°$. In contrast, for T_4A_4GC the bending direction is distributed more uniformly over the entire interval α = (0,360°) and the preference for bending at α = 270° is much less pronounced than the peak at α = 90° for A_4T_4CG. This difference becomes understandable if we turn to the circle diagrams of Fig. 4

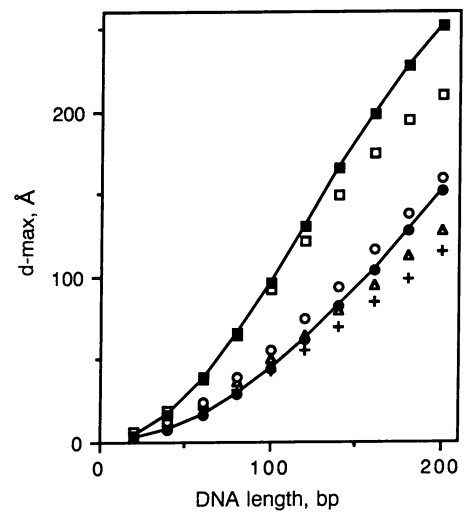

FIG. 5. "Width" of the curved DNA d-max (40), as a function of DNA length. Solid symbols (connected by lines) are for the static models of A_4T_4CG (■) and T_4A_4GC (●), respectively. Unconnected open symbols are for the MC ensemble of DNA fragments. □, A_4T_4CG; ○, T_4A_4GC; △, $(AG)_5$·$(CT)_5$; +, $A_{10}T_{10}$. The decamers were generated with periodic boundary conditions. The Boltzmann distribution obtained was used to generate longer pieces of DNA. Shown are the averages for 5 × 10^4 chains. The rms deviations for 200 bp are 33 Å and 52 Å for A_4T_4CG and T_4A_4GC, respectively.

again. In A_4T_4CG the local bending vectors are localized predominantly in the lower part of the diagram, and their fluctuations do not change the general trend in the decamer bending; whereas in T_4A_4GC these vectors are directed both up and down, their sum is close to zero, and thus fluctuations influence the direction of bending dramatically. This leads to serious consequences in terms of the overall shape of the long fragments of DNA.

Comparison of static DNA segments with the MC-generated ("flexible") segments shows that for A_4T_4CG the former are curved more strongly than the latter: d-max for the static segments is larger than for the flexible segments (Fig. 5), whereas the end-to-end distance is larger for the flexible segments of 150–200 bp (data not shown). We interpret these data assuming that fluctuations "blur" sharp curvature of the long pieces of DNA. On the other hand, when the T_4A_4GC decamers from the MC ensemble are "ligated," the resulting segments become shorter and broader than the segments formed from the identical decamers (see d-max values in Fig. 5). So, the static model predicts the larger difference between the strongly and slightly curved segments of DNA than does the MC sampling.

One more result, derived from Fig. 5, is that the slightly curved DNA sequence GT_4A_4C, for which bending angle β_s = 6°, has practically the same shape as the intrinsically straight but thermally bent sequences poly(dA)·poly(dT) and poly(dA-dG)·poly(dC-dT). This can explain the relative insensitivity of the polyacrylamide gel matrix to small degrees of DNA curvature (4, 41). Note that the smallest d-max value for poly(dA)·poly(dT) is consistent with the increased gel mobility in this case (4).

DISCUSSION

The phenomenon of DNA curvature is essentially statistical in nature (3, 8, 42), and the static model can be considered only as a first approximation. For periodic sequences the differences between the two approaches can be demonstrated by comparing the values of β, the average bending angle per decamer, and β_s, the vectorial sum of the average local bends. For the sequences with the strong curvature $\beta \approx \beta_s$;

however, when the curvature is less pronounced (e.g., in A_5T_5 and T_4A_4GC), the two values differ significantly: $\beta_s << \beta$. In addition, for the same average roll and tilt angles, the static approach gives a much greater difference in the shape of the curved and straight molecules than does the statistical approach (Fig. 5). It happens because $\beta_s = 0$ for the static model of the straight DNA, but $\beta \approx 15°$ for the MC ensemble [see $(AG)_5 \cdot (CT)_5$ and $A_{10} \cdot T_{10}$ in Table 1]. Therefore, comparisons between the curved and straight DNA are made against this background.

So, the static model overestimates the difference between the "straight" and "curved" DNA, but underestimates deflection of axis of the "slightly curved" sequences from the straight line. Therefore, certain readjustments of the wedge values (5, 6) are necessary for any quantitative comparison with the electrophoretic data on DNA curvature. Namely, the statistically averaged wedge angles are probably larger than estimated on the basis of the static model (6); this was shown to be especially true for the roll in TA·TA and CA·TG dimers (Fig. 2).

We have simulated $A_n \cdot T_n$ blocks, using the NMR restrictions for the interproton distances (24, 25) and thus implicitly taking into account stabilization of $A_n \cdot T_n$ by the hydration spine (22, 23). Within the framework of this model, A_n runs appear to be more rigid than the other sequences. However, even in the absence of the NMR restrictions, flexibility of oligo(dA)·oligo(dT) is less pronounced than that of alternating $(AG)_n \cdot (CT)_n$ (26). This result implies that other factors, such as large propeller and buckle angles, interaction of the thymine methyl group with the neighboring sugar ring, and bifurcated hydrogen bonds might also be partly responsible for the relative stiffness of the $A_n \cdot T_n$ tracts (26).

Performing MC calculations by sampling generalized internal coordinates, we have been able to analyze the sequence-dependent bending of DNA at different levels of resolution. By increasing the length of the DNA segment over which the "segmental averaging" is performed, from 2 to 5 to 10 bp, we are progressing from variations in the DNA geometry at the base step level (roll angles in Fig. 2) to the middle range variation of the minor groove size (Fig. 3) and on toward more macroscopic representations of DNA bending (Figs. 1 and 4).

The strongest curvature of DNA in solution is detected for periodically repeating $A_n \cdot T_n$ runs, and the singular deflections of the DNA axis in certain dimers are shown to be less important (11, 12). In particular, these findings disfavor the pyrimidine–purine mechanism of bending (8, 32) proposed initially to explain curvature of the kinetoplast DNA. In accord with electrophoretic data (11, 12, 36, 37), our MC simulations show that cumulative gradual rolling of several consecutive AA·TT dimers does produce much stronger effect than isolated pyrimidine–purine rolls (Fig. 2 and Table 1). However, in the protein–DNA complexes, where presumably the local bend angles are larger and fluctuations are more restricted than in free DNA, the pronounced rolls [kinks or minikinks (8, 13)] in CA·TG and TA·TA dimers appear to be a major origin of DNA bendability (30, 43, 44). This indicates that different impacts of the two types of DNA bending (gradual and singular) should be expected for free DNA in solution compared to the complexes with proteins.

Note Added in Proof. In agreement with our data in Fig. 3, M. A. Price and T. D. Tullius have shown that the maximum in the hydroxyl cleavage pattern for A_5T_5 is shifted downstream by two to three nucleotides with respect to A_5X_5 (poster presented at the Seventh Conversation in Biomolecular Stereodynamics, June 18–22, 1991, Albany, NY).

We are grateful to Drs. V. I. Ivanov, G. G. Malenkov, and E. N. Trifonov for the valuable discussions, to W. K. Olson for the critical remarks, and to Drs. K.-L. Ting, P. Greif, and D. Covell for help. This research was sponsored, at least in part, by the National Cancer Institute under Contract NO1-CO-74102 with Program Resources, Inc., and Institute of New Technologies, Moscow.

1. Trifonov, E. N. (1985) *CRC Crit. Rev. Biochem.* **19**, 89–106.
2. Crothers, D. M., Haran, T. E. & Nadeau, J. G. (1990) *J. Biol. Chem.* **265**, 7093–7096.
3. Hagerman, J. P. (1990) *Annu. Rev. Biochem.* **59**, 755–781.
4. Koo, H.-S. & Crothers, D. M. (1988) *Proc. Natl. Acad. Sci. USA* **85**, 1763–1767.
5. De Santis, P., Palleschi, A., Savino, M. & Scipioni, A. (1990) *Biochemistry* **29**, 9269–9273.
6. Bolshoy, A., McNamara, P., Harrington, R. & Trifonov, E. (1991) *Proc. Natl. Acad. Sci. USA* **88**, 2312–2316.
7. Schellman, J. A. (1974) *Biopolymers* **13**, 217–226.
8. Ulyanov, N. B. & Zhurkin, V. B. (1984) *J. Biomol. Struct. Dyn.* **2**, 361–385.
9. Srinivasan, A. R., Torres, R., Clark, W. & Olson, W. K. (1987) *J. Biomol. Struct. Dyn.* **5**, 459–496.
10. Sarai, A., Mazur, J., Nussinov, R. & Jernigan, R. L. (1989) *Biochemistry* **28**, 7842–7849.
11. Diekmann, S. (1986) *FEBS Lett.* **195**, 53–56.
12. Koo, H.-S., Wu, H.-M. & Crothers, D. M. (1986) *Nature (London)* **320**, 501–506.
13. Zhurkin, V. B., Lysov, Yu. P. & Ivanov, V. I. (1979) *Nucleic Acids Res.* **6**, 1081–1096.
14. Ulyanov, N. B. & Zhurkin, V. B. (1982) *Molek. Biol. (Engl. transl.)* **16**, 857–867.
15. Metropolis, N. A., Rosenbluth, A. W., Rosenbluth, M. N., Teller, A. H. & Teller, E. (1953) *J. Chem. Phys.* **21**, 1087–1092.
16. Hagerman, P. S. (1986) *Nature (London)* **321**, 449–450.
17. EMBO Workshop (1989) *EMBO J.* **8**, 1–4.
18. Zhurkin, V. B., Lysov, Yu. P. & Ivanov, V. I. (1978) *Biopolymers* **17**, 377–412.
19. Zhurkin, V. B., Poltev, V. I. & Florent'ev, V. L. (1981) *Molek. Biol. (Engl. transl.)* **14**, 882–895.
20. Poltev, V. I. & Shulyupina, N. V. (1986) *J. Biomol. Struct. Dyn.* **3**, 739–765.
21. Zhurkin, V. B., Lysov, Yu. P., Florentiev, V. L. & Ivanov, V. I. (1982) *Nucleic Acids Res.* **10**, 1811–1830.
22. Lipanov, A. A. & Chuprina, V. P. (1987) *Nucleic Acids Res.* **15**, 5833–5844.
23. Chuprina, V. P. (1987) *Nucleic Acids Res.* **15**, 293–310.
24. Nadeau, J. G. & Crothers, D. M. (1989) *Proc. Natl. Acad. Sci. USA* **86**, 2622–2626.
25. Katahira, M., Sugeta, H. & Kyogoku, Y. (1990) *Nucleic Acids Res.* **18**, 613–618.
26. Zhurkin, V. B., Gorin, A. A., Charakhchyan, A. A. & Ulyanov, N. B. (1990) in *Theoretical Biochemistry and Molecular Biophysics*, eds. Beveridge, D. L. & Lavery, L. (Adenine, Guilderland, NY), Vol. 1, pp. 411–431.
27. Singh, U. C., Weiner, S. J. & Kollman, P. (1985) *Proc. Natl. Acad. Sci. USA* **82**, 755–759.
28. Frank-Kamenetskii, M. D., Lukashin, A. V., Anshelevich, V. V. & Vologodskii, A. V. (1985) *J. Biomol. Struct. Dyn.* **2**, 1005–1012.
29. Levene, S. D. & Crothers, D. M. (1986) *J. Mol. Biol.* **189**, 73–83.
30. McNamara, P. T., Bolshoy, A., Trifonov, E. N. & Harrington, R. E. (1990) *J. Biomol. Struct. Dyn.* **8**, 529–538.
31. Arnott, S. (1972) in *The Purines: Theory and Experiment*, Proceedings of the 4th Jerusalem Symposium, eds. Bergman, E. D. & Pullman, B. (Israel Acad. of Sci. and Humanities, Jerusalem), pp. 102–110.
32. Hagerman, P. J. (1984) *Proc. Natl. Acad. Sci. USA* **81**, 4632–4636.
33. Ulanovsky, L. & Trifonov, E. (1987) *Nature (London)* **326**, 720–722.
34. Ulanovsky, L., Bodner, M., Trifonov, E. & Choder, M. (1986) *Proc. Natl. Acad. Sci. USA* **83**, 862–866.
35. Koo, H.-S., Drak, J., Rice, J. A. & Crothers, D. M. (1990) *Biochemistry* **29**, 4227–4234.
36. Hagerman, P. S. (1988) in *Unusual DNA Structures*, eds. Wells, R. D. & Harvey, S. C. (Springer, New York), pp. 225–236.
37. Shlyakhtenko, L. S., Lyubchenko, Yu. L., Chernov, B. K. & Zhurkin, V. B. (1990) *Molek. Biol. (Engl. transl.)* **24**, 66–81.
38. Burkhoff, A. M. & Tullius, T. D. (1987) *Cell* **48**, 935–943.
39. Fratini, A. V., Kopka, M. L., Drew, H. R. & Dickerson, R. E. (1982) *J. Biol. Chem.* **257**, 14686–14707.
40. Tung, C.-S. & Burks, C. (1987) *J. Biomol. Struct. Dyn.* **4**, 553–559.
41. Diekmann, S. & von Kitzing, E. (1988) in *Structure and Expression*, eds. Olson, W. K., Sarma, M. H., Sarma, R. H. & Sundaralingam, M. (Adenine, Guilderland, NY), Vol. 3, pp. 57–67.
42. Zhurkin, V. B., Ulyanov, N. B. & Ivanov, V. I. (1988) in *Structure and Expression*, eds. Olson, W. K., Sarma, M. H., Sarma, R. H. & Sundaralingam, M. (Adenine, Guilderland, NY), Vol. 3, pp. 169–190.
43. Steitz, T. A. (1990) *Q. Rev. Biophys.* **23**, 205–280.
44. Barber, A. M. & Zhurkin, V. B. (1990) *J. Biomol. Struct. Dyn.* **8**, 213–232.